Low-Cost Inkjet-Printed Fully Passive RFID Tags for Calibration-Free Capacitive/Haptic Sensor Applications

Sangkil Kim, *Student Member, IEEE*, Yoshihiro Kawahara, *Member, IEEE*, Apostolos Georgiadis, *Senior Member, IEEE*, Ana Collado, *Senior Member, IEEE*, and Manos M. Tentzeris, *Fellow, IEEE*

***Abstract*— A fully passive, compact, and low-cost capacitive wireless radio frequency identification (RFID)-enabled sensing system for capacitive sensing and other Internet of Things applications is proposed. This calibration-free sensor utilizes a dual-tag topology, which consists of two closely spaced RFID tags with dipole antennas and printed capacitive sensor component connected to one of the tags. A series LC resonator is used to both reduce the antenna size and improve the isolation between the two antennas and the design/optimization steps are discussed in detail. All components except for the RFID chips are inkjet printed on an off-the-shelf photopaper using a silver nanoparticle ink. The complete sensor dimension is 84 mm × 95 mm and the sensor is compatible with EPC Class 1 Gen 2 (UHF) standard reader technology at 915 MHz.**

***Index Terms*— Capacitive sensing, cross-talk suppression, differential sensing, inkjet-printing technology, Internet of Things (IoT), remote sensing, RFID-enabled sensor, RFID, wireless sensors, haptic sensors.**

I. Introduction

OVER the last decade radio frequency identification (RFID)-enabled sensing systems have received an increasing level of attention mostly due to their relative simple system architecture, that typically consist of simple sensing tags and interrogation readers facilitating their integration with other existing Wireless Sensor Networks (WSN) and RFID infrastructure [1]. In addition, a passive RFID sensing system's life time is longer and its cost is much lower compared to active sensing systems, while RFIDs can constitute low-power wireless platforms [2] with broad sensing capabilities including temperature, gas, strain and humidity sensing [3]–[6]. For example, electronics utilizing low-power RFID-enabled motion sensors can be turned on at user's presence or need, which leads to energy saving. It is also possible to utilize such sensor systems as a smart skin for strain, ambient conditions and biomonitoring sensing applications or a bio-monitoring sensor as well as a Machine-to-Machine (M2M) communication node when it is integrated to the WSNs [7]–[9]. Plus, the RFID-enabled sensor systems could potentially be one of the most enabling factors to implement realistic large-scale topologies of Internet of things (IoT) in the future [10].

Reported works demonstrated feasibility and capability of the RFID-enabled sensors. In [21], two dipole antennas were printed on paper substrate and a sensor tag had a printed resistive sensor. The resistance of the resistive sensor changes as the sensor absorbs the moisture. In [22], two ordinary RFID tags were utilized while one of them was covered with a water-absorbing material. Those reported works are measuring the required minimum transmitted (Tx) power to detect the moisture content of the ambient environment based on the dual-tag sensing topology. However, those reported sensor systems work at high relative humidity value more than 70 % to get a notable signal difference between the sensor and the reference tags while having a larger size compared to the proposed design in this paper. The size of the reported sensor tag is 37 % smaller than the reported RFID-enabled sensor tag in [21]. In this paper, an inkjet-printed RFID-enabled haptic sensor utilizing a dual-tag sensing topology on paper substrate is presented. Preliminary results of a prototype sensor tag and a proof-of-concept demonstration of the differential sensing architecture were presented in [11]. This paper additionally includes the parametric analyses used to optimize the size and performance of the sensor, while discussing a theoretical estimation of the range of the dual-tag sensor, and an event-detection method based on the statistical processing of the sensor response versus frequency.

Nevertheless, there are still numerous challenges on implementing the proposed RFID-enabled sensor with the dual tag sensing topology. First of all, the crosstalk between

Manuscript received August 5, 2014; revised October 24, 2014; accepted October 31, 2014. Date of publication November 3, 2014; date of current version April 16, 2015. The work of S. Kim and M. M. Tentzeris was supported by the National Science Foundation and the New Energy and Industrial Technology Development Organization (NEDO). The work of Y. Kawahara was supported by the NEDO. The work of A. Georgiadis and A. Collado was supported by the Spanish Ministry of Economy and Competitiveness under Project TEC2012-39143, and by the European Union Marie Curie under Project FP7-PEOPLE-2009-IAPP 251557. The associate editor coordinating the review of this paper and approving it for publication was Prof. Madhusudan Singh.

S. Kim and M. M. Tentzeris are with the School of Electrical and Computer Engineering, Georgia Institute of Technology, Atlanta, GA 30332 USA (e-mail: ksangkil3@gatech.edu; etentze@ece.gatech.edu).

Y. Kawahara is with the University of Tokyo, Tokyo 113-8654, Japan (e-mail: kawahara@akg.t.u-tokyo.ac.jp).

A. Georgiadis and A. Collado are with the Centre Tecnologic de Telecomunicacions de Catalunya, Barcelona 08860, Spain (e-mail: ageorgiadis@cttc.es; ana.collado@cttc.es).

Color versions of one or more of the figures in this paper are available online at http://ieeexplore.ieee.org.

Digital Object Identifier 10.1109/JSEN.2014.2366915

the multiple tags utilized in the sensor should be considered. A higher amount of power is required to activate the dual-tag sensor compared to typically used single-tag sensor topologies since multiple RFID IC's should be activated by the reader, otherwise same amount of interrogation power result in shorter reading ranges. It is important to find an optimal distance between the two dipole antennas in order to minimize the size of the sensor as well as the crosstalk level, thus preventing unwanted power losses. The cost of the RFID-enabled sensor is also a critical factor for large-scale practical implementations.

In this paper, an antenna-embedded series inductor-capacitor (LC) resonator and inkjet printing technology are employed to address the aforementioned design challenges. The LC resonator has been integrated into the RFID antennas not only to suppress the crosstalk between the antennas but also to reduce the antenna size [12], [13]. The inkjet printing method was utilized as a fabrication method in this paper in order to take advantages of low-cost, scalable and variable properties of the printing technology [14], [15]. This paper presents a miniaturized RFID-enabled sensor tag using the printed LC-resonator loaded dipole antenna in reducing the spacing of the sensing tag and the reference tag and provides theoretical insights on design the dual-tag RFID-enabled sensor. The statistical method was utilized to provide robust detection of the event which can be applied to any other dual-tag RFID-enabled sensor topology.

In Section II, the design procedure of the RFID-enabled sensor with the series LC resonator is presented in detail covering the single/dual tag sensing topology, the series LC resonator, and the design rules for the level system integration, as well as a theoretical estimate for the reading range. In Section III, the measured experimental results and an "event-occurrence" decision technique.

II. RFID-Enabled Sensor Design With LC Resonator

A. Dual-Tag Sensing Topology

There are two types of passive RFID-enabled sensing topologies: single-tag sensing and dual-tag sensing. The basic concept of those RFID-enabled sensing topologies is introduced in Fig. 1. The single-tag topology utilizes one RFID tag integrated with an inductive or a capacitive sensing component [5], [16] or the sensing capability is implemented on RFID chip [17]–[20]. The backscattered signal from a sensor tag experiences changes, such as frequency shift or modulation, in the event of the detection of different quantities of a sensed parameter. The difference quantities affect the impedance of the RFID antenna-sensor combination, as shown in Fig. 1(a).

This type of RFID-enabled sensor topology is relatively easy to implement due to the simplicity of the sensor system. However, the resonant frequency of the RFID antenna or a sensing component can also be affected by its surrounding environment. It results in an unwanted shift of the resonant frequency of the sensor tag or a false alarm when the RFID antenna is utilized as a sensor. In this case, it is hard to determine if the sensing event detection from the sensor tag is true or false and a typically cumbersome calibration process has to be implemented.

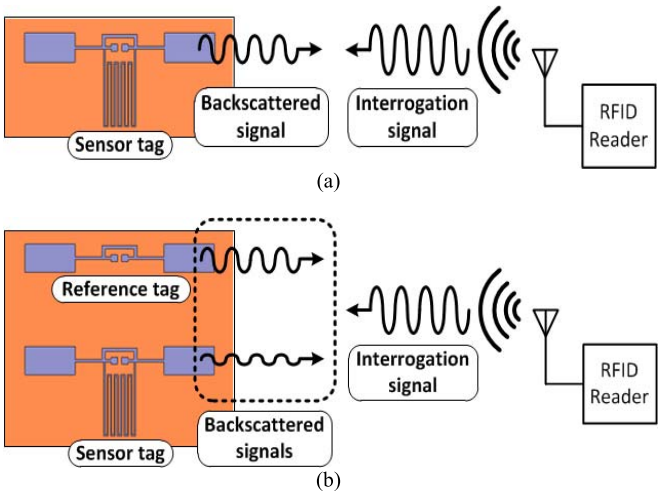

Fig. 1. RFID-enabled sensor topologies: (a) single-tag and (b) dual-tag sensing topology.

Unlike the single RFID tag sensing system, the dual-tag sensing topology utilizes two RFID tags (a sensor tag and a reference tag) for a calibration-free detection and decision process as shown in Fig. 1(b) [6], [21], [22]. A reader can distinguish two tags because each RFID chip of the tag returns their identification code when a tag is excited. The sensing tag of the dual-tag sensing topology is similar to the sensing tag of the single tag sensing topology while the reference tag is an identical RFID tag excluding the sensing component. The individual backscattered/response signals from the two tags of the dual sensor tag configuration are almost identical when no sensing event is detected. The response of the two tags becomes different when a sensing event is triggered (e.g. in the presence of a sensed substance), and a decision process can be defined by comparing the backscattered signals from the two tags. This type of sensing topology is operating in a robust way compared to the single-tag sensing system because the event decision is made utilizing the difference of the backscattered signals between the sensor tag and the reference tag or the backscattered signal from the reference tag as a calibration signal. Therefore, the effects of unwanted reflections from surrounding objects and of different mounting substrates can be easily calibrated out. However, introducing an additional reference tag increases the total size of the sensor and may also cause crosstalk issues between the individual tags. The crosstalk level typically increases as the distance between the sensor tag and reference tag decreases, which commonly results in short read range and poor readability due to increased minimum required power to activate the passive dual sensor tag. Therefore, when designing a dual-tag sensor, it is important to find the optimum distance between the two antennas (sensor tag and reference tag) in order to satisfy simultaneously the requirements of a minimal crosstalk level and of a miniaturized size. The reported single and dual tag RFID-enabled sensors were summarized in Table I.

TABLE I
RFID-ENABLED SENSORS

	[21]	[22]	[6]	Proposed Work
Operation Frequency (MHz)	915	868 & 2450	880 ~ 903	820 ~ 940
Sensor Topology	Dual Tag	Dual Tag	Single Tag	Dual Tag
Sensor Size (mm^2)	188 × 58	103 × 226	106 × 39	89 × 58
Ant. to Ant. Distance (mm)	58	206	N/A	45
Type	Moisture	Moisture	Moisture	Touch

B. Isolation Structure: Series LC Resonator

In this paper, an isolation structure consisting of a series LC resonator is utilized in order to both suppress the crosstalk level and reduce the spacing between the two RFID tags [23], [24]. In this paper, LC resonator structures that consist of a thin-strip inductor and an interdigitated capacitor [23], [24] are introduced in the RFIDs' dipole antennas as shown in Fig. 2. The unit inductance of a flat rectangular line has been reported in [25] showing that its width is the dominant design parameter when its metal thickness is much smaller than the width. The full wave 3D simulator, Ansys HFSS v11.1, is utilized for this analysis. The crosstalk level variation as a function of the width (W_L) of the inductor line while fixing the design parameters of the interdigitated capacitor ($W_C = 0.1$ mm, $L_C = 2.0$ mm) is shown in Fig. 3(a). The crosstalk level between the antenna 1 and antenna 2 in Fig. 2(b) is shown in terms of S_{21} for a fixed distance between the antennas of $d = 45$ mm. Its variation versus the changes of the unit inductance of the isolator is relatively small compared to the variation of the crosstalk level versus the capacitance change as shown in Fig. 3(a), (b). Based on the analysis shown in Fig. 3, the most important design parameters are the width and the gap of the interdigitated capacitor (W_C) compared to the length of the fingers (L_C) as the fringing capacitance plays a significant role in the value of the total capacitance [26]. Given the area of the patch termination of the RFIDs' dipole antennas, the dimensions of the LC resonator are chosen to minimize the crosstalk level ($W_L = 0.4$ mm, $W_C = 0.1$ mm, $L_C = 2.0$ mm) which results in 29 fingers of the interdigitated capacitor. The L_C resonators are placed asymmetrically along the dipole axis (X-axis) to induce out-of-phase near-field current to suppress mutual coupling [24]. The overall size of the proposed sensor tag is 77×90 mm^2 (69.3 cm^2) including the sensing component which is 37 % smaller than the reported RFID-enabled sensor tag that has a size of 58×188 mm^2 (109.04 cm^2) [21].

C. RFID-Enabled Sensor Tag With LC Resonators

The smallest distance value (d) between the antennas is chosen in order to minimize the total size of the RFID-enabled sensor tag while satisfying the desired crosstalk level at the operation frequency range. In this paper, the crosstalk level of −25 dB throughout the bandwidth of operation (850-950 MHz) is chosen as a design example. The two RFID tags with the dipole embedded LC resonator are placed side-by-side. The distance (d) of 45 mm ($0.137\lambda_0$) is chosen and the crosstalk level without the isolation structure (series LC resonator) is shown in Fig. 4 as a reference. The crosstalk level of the antennas with the isolator is about 4 ~ 5 dB lower than the antennas without the isolator at the operation frequency range. The operation principle of the proposed tag, described in detail in Section III, is dependent on the capability of each antenna to operate independently from the other one, and therefore, suppressing the crosstalk level between the antennas is an important task of this paper. The length of the RFID antennas is also miniaturized due to the loaded LC resonator. The length of the proposed inkjet-printed antenna on paper substrate is 89.2 mm ($0.27\lambda_0$) which is 28.4 % shorter than the length of the inkjet-printed dipole antenna on paper substrate without any miniaturization (125 mm, [27]) at the operation frequency of 915 MHz.

The final design step involves the integration of a sensing/event detecting meandered line with the antenna of the sensing tag, featuring a frequency response that is dependent on

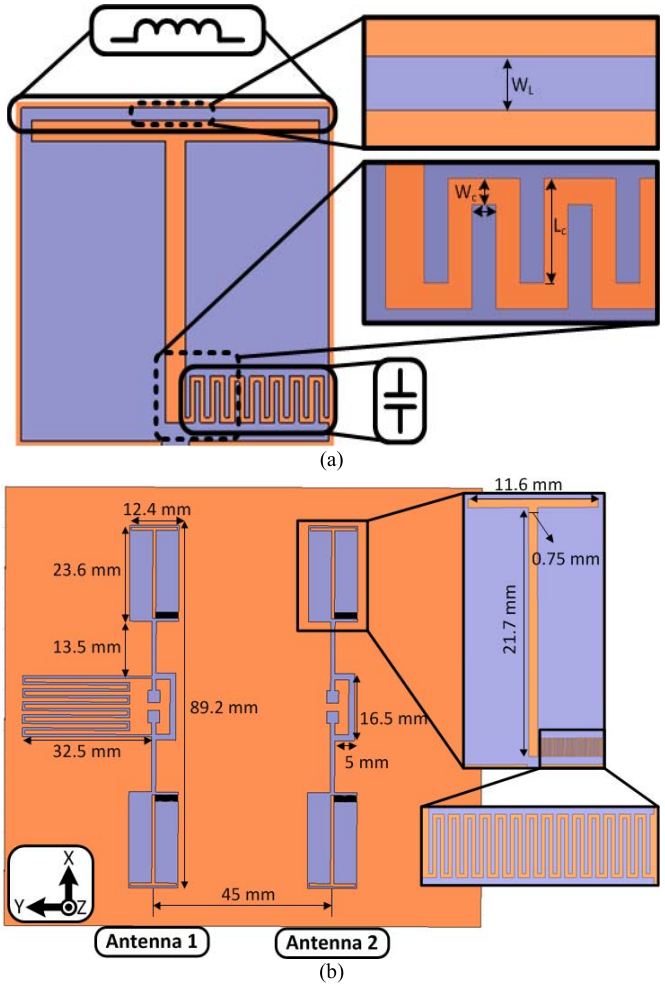

Fig. 2. (a) Structure of the LC resonator and (b) a geometry of the proposed RFID-enabled sensor.

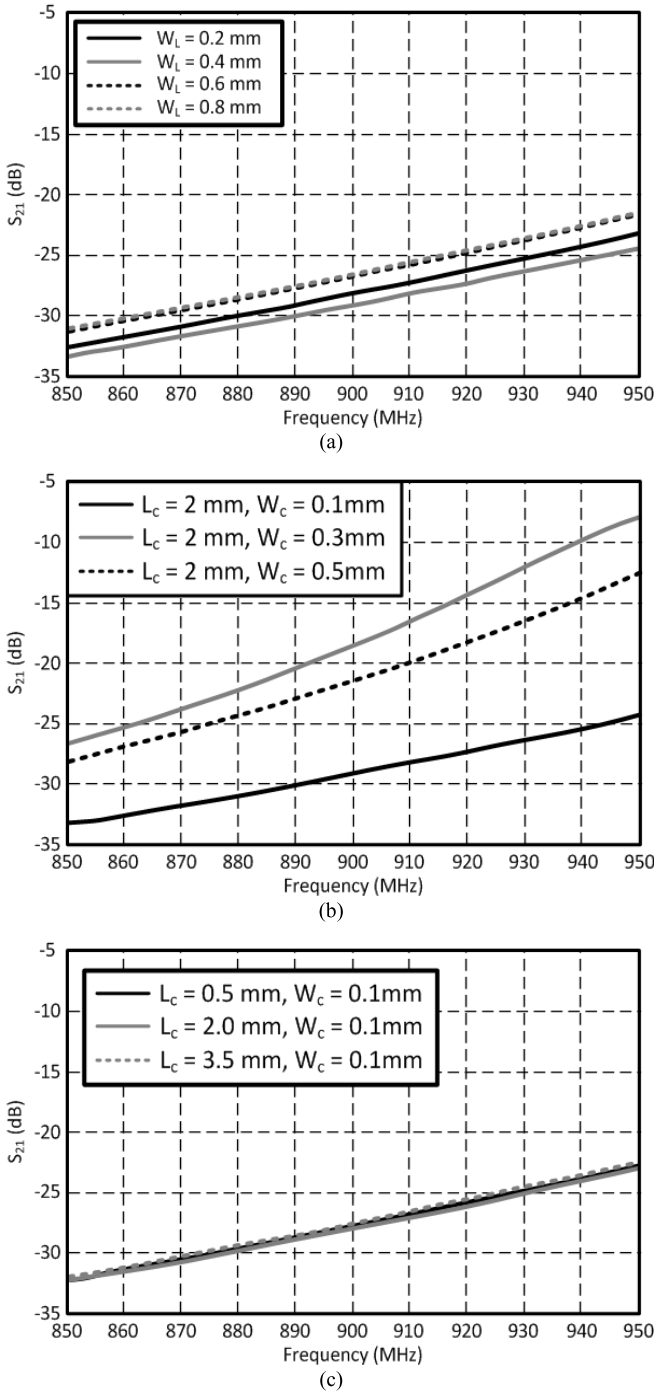

Fig. 3. Parameter sweep of the LC resonator structure: (a) width (W_L) of the inductor, (b) width (W_c) and (c) length (L_c) of the interdigitated capacitor.

the presence of the sensing target. The size of the proposed RFID-enabled sensor including the meandered line is 84 mm × 95 mm. The antenna with the meandered line is the sensing configuration with a frequency response depending on the presence of the sensing target. The meandered line should not affect the antenna's resonant frequency while at the same time it should be sensitive enough to be able to sense the target event. The meandered line is designed to have the high impedance at the resonant frequency of the antenna by optimizing the width (inductance) and the pitch

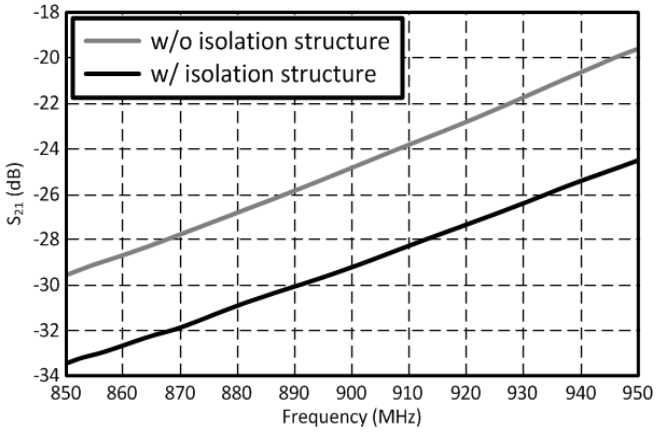

Fig. 4. Crosstalk level between the antenna 1 and the antenna 2 with/without the LC resonators.

(capacitance) of the meandered line [28]. Thus, it is designed to feature a high impedance (open-circuit) in the absence of a sensing event and a gradually lower impedance value eventually affecting the resonant frequency of the sensing tag in the presence of a sensing target. The optimal value for the width of the meander line is 0.6 mm and the pitch of the line is 3.2 mm and the detailed dimensions of the proposed RFID-enabled sensor are shown in Fig. 2(b).

The resonant frequency of the sensor tag (antenna 1 in Fig. 2(b)) is strongly affected by the capacitance variation of the sensing meandered line (capacitive sensing) due to the loading effect when a high dielectric constant (ε_r) and loss tangent (tan δ) material, such as a human finger (haptic sensing), approaches or touches the meandered line. The peak frequency of the reference tag's (antenna 2 in Fig. 2(b)) S_{11} curve is also shifted due to the change of the mutual impedance when the human finger acts as an additional load to the sensor tag resulting in a different matching point. Initially (lack of the finger presence) the two antennas have similar frequency responses (S_{11} (antenna 1) & S_{22} (antenna 2)) before the human finger touches the meandered line (no event). The resonant frequencies of the antenna 1 and the antenna 2 are 928 MHz and 911 MHz, respectively. The resonant frequency of the sensor tag (antenna 1) is shifted to a lower frequency (885 MHz) due to the loading (higher capacitance) effect of a touching finger (event occurrence) although the reference tag (antenna 2) keeps almost the same resonant frequency (920 MHz). In our benchmarking case, the resonant frequency of the sensor tag shifted by 43 MHz while that of the reference tag shifted by 9 MHz as shown in Fig. 5. The human finger has been modeled as a rectangular box which has the dielectric constant (ε_r) of 21.14 and the conductivity of 0.36 S/m. The values of the dielectric constant and the conductivity were chosen to the mean values of those of the human skin, the flesh, and the bone [29]. The RFID chip (NXP's SL3ICS1002/1202 [30]) is modeled as a parallel resister-capacitor (R-C) network to model the frequency dependence of the input impedance of the chip. The modeled resister value (R) is 1.13 kΩ and the capacitance value (C) is 1.41 pF which results in the input impedance of 13.3−j122 Ω at 915 MHz. At 915 MHz, the magnitudes of the reflection coefficients of

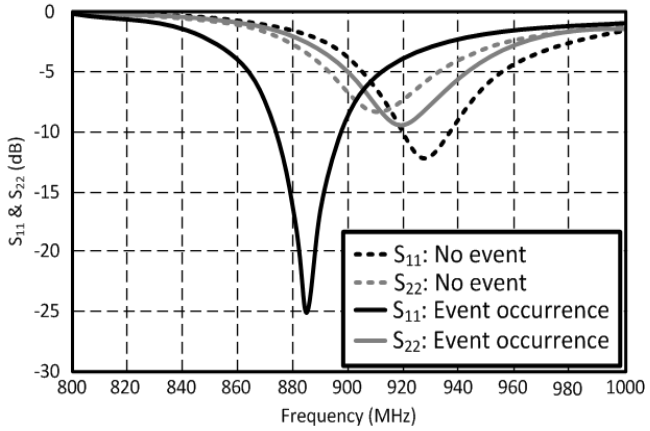

Fig. 5. Simulated scattering parameters (S_{11} and S_{22}) of the sensor tag (antenna 1) and the reference tag (antenna 2).

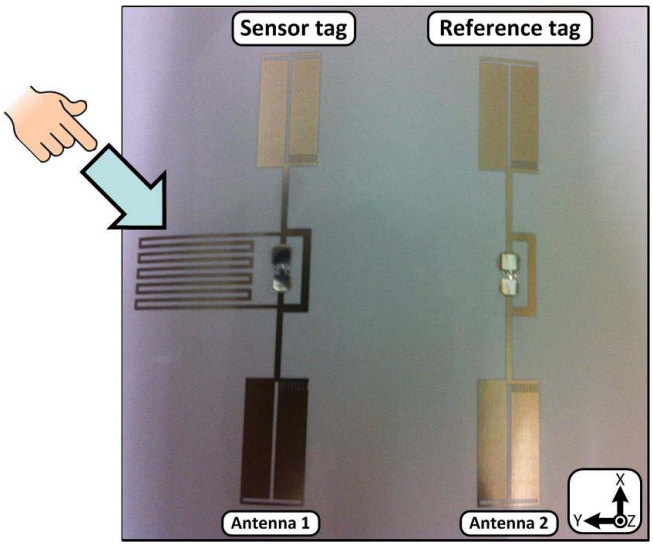

Fig. 6. Inkjet-printed RFID-enabled sensor on paper substrate.

the antenna 1 (S_{11}) and the antenna 2 (S_{22}) are −8.11 dB and −8.13, respectively. However they get different after the event occurrence (S_{11}: −4.54 dB and S22: −9.02 dB), which results in two different required transmitted (Tx) power curves to excite each tag over the simulated frequency range, that can be utilized to make an event decision (Section III-B).

D. Read Range Estimation

Fig. 6 shows the inkjet-printed RFID-enabled sensor on paper and Fig. 7 shows the simulated radiation patterns of the designed RFID-enabled single and dual tag sensors along the E- (XZ) and H- (YZ) planes. The patterns are normalized by that of the reference tag. In the case of the dual tag sensor, the radiation patterns of each tag antenna are plotted by exciting one antenna while leaving open the other. Furthermore, Fig. 7 includes the radiation patterns of the dual tag sensor when a human finger touches the sensor tag. It can be observed that both the single and dual tag sensors have similar radiation patterns with an omni-directional shape. The individual gain values of the antennas of the dual-tag sensor are 3.3 dBi (sensing tag antenna) and 3.71 dBi (reference tag antenna) at 915 MHz, which become 0.0 dBi (sensing tag antenna) and

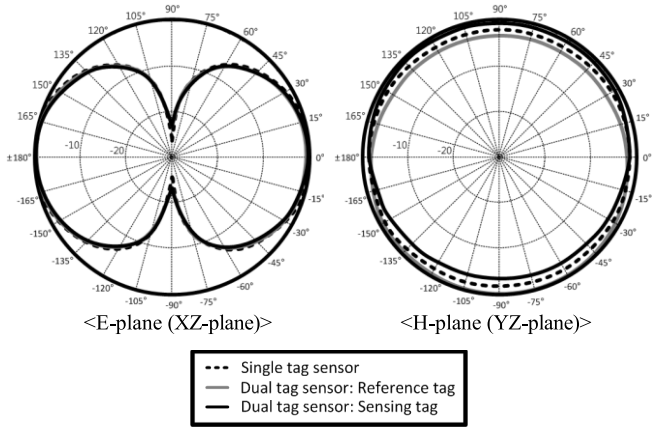

(a)

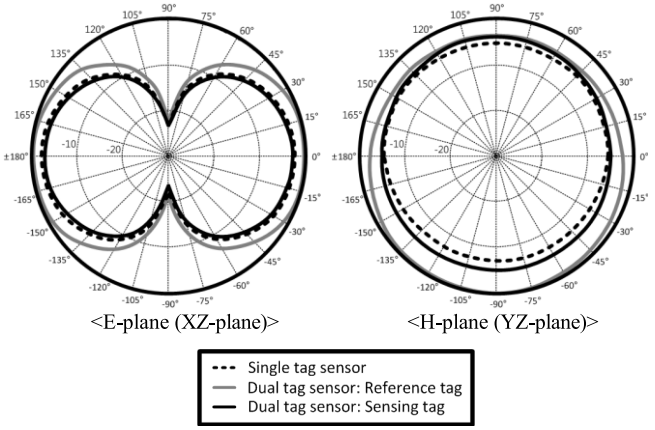

(b)

Fig. 7. Calculated radiation patterns of the RFID-enabled single-tag and double-tag sensors (a) without touch and (b) with touch.

3.47 dBi (reference tag antenna) when a human finger touches the sensor. In comparison the single tag sensor demonstrated a gain of 1.94 dBi at 915 MHz for the single tag sensor, which became −1.21 dBi when a human finger touches the sensor.

The read range of a single antenna tag can be estimated using (1) based on the antenna gain values, the input impedance of the antenna, and the impedance of the RFID chip, using Friis free-space transmission formula as shown in [31]. The estimated theoretical read range based on the measurement is shown in Fig. 8. The measured minimum required Tx power to read the both tags (sensor tag and the reference tag) were used to calculate the read range of the sensor tag. The maximum read range is about 2.6 m at 915 MHz before the event occurrence while the read range after the event occurrence is about 1.6 m at 915 MHz due to the decreased gain of the sensor tag as shown in Fig. 9 which limits the read range.

$$R = \frac{\lambda_0}{4\pi}\sqrt{\frac{P_t G_t G_r \tau}{P_{th}}} \tag{1}$$

$$\tau = \frac{4R_a R_c}{|Z_c + Z_a|^2} \tag{2}$$

where λ_0 is the wavelength in the free-space, P_t is the transmitted power by the reader, G_t is the gain of the transmitting

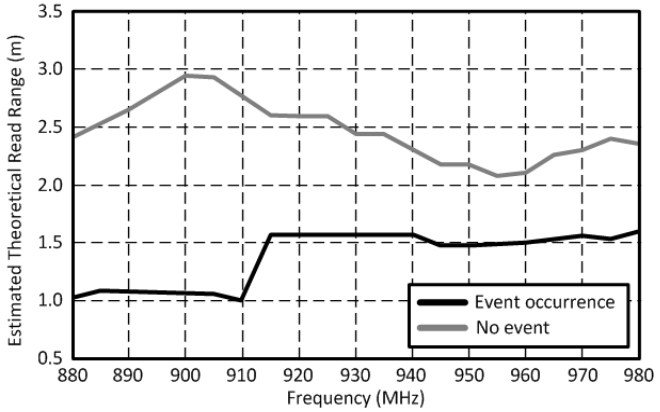

Fig. 8. Estimated theoretical read range.

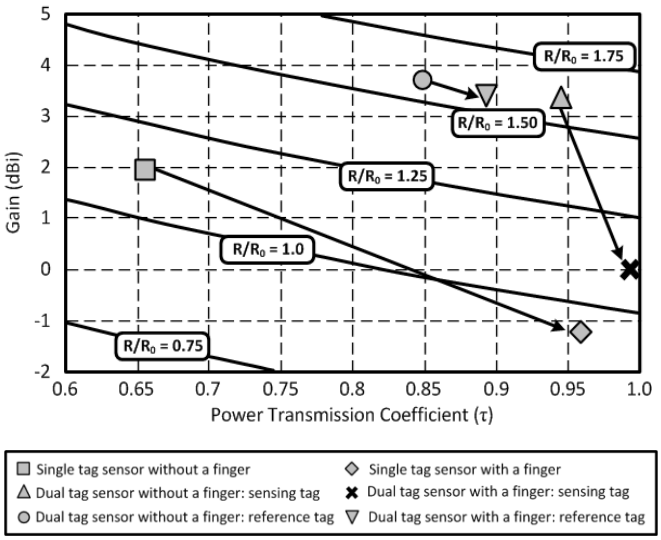

Fig. 9. Read range of the RFID-enabled sensor tags at 915 MHz.

antenna of the reader, G_r is the gain of the receiving RFID tag antenna, P_{th} is the minimum required power to excite the RFID chip, and τ is the power transmission coefficient [31]. $Z_c = R_c + jX_c$ and $Z_A = R_A + jX_A$ are the complex impedances of the RFID chip and the antenna, respectively. The read range R of an RFID tag is proportional to the square root value of the transmitted power P_t as shown in (1), because the other parameters such as the wavelength, the gain of the Tx and Rx antennas, the threshold power level to excite a RFID chip P_{th}, and the power transmission coefficient τ [30] are fixed once the antenna measurement system is established at each interrogation frequency. The range equation (1) can be normalized to a reference range factor,

$$R_0 = \frac{\lambda_0}{4\pi}\sqrt{\frac{P_t G_t}{P_{th}}} \tag{3}$$

R_0 is the estimated range of a tag which has a gain of 0 dBi and which is matched to the RFID chip at the operation frequency. The normalized range (1) can therefore be written as,

$$\frac{R}{R_0} = \sqrt{G_r \tau} \tag{4}$$

In the case of a two port system such as the dual tag sensor or generally a multiport system, the formulation needs to be modified to reflect the fact that the received power at each antenna is affected by the mutual coupling among the different antennas. The theory of loaded multiport scatterers has been presented in [32]. The theory of [32] combined with reciprocity theory [33] was used in [34] to optimize the RF-DC conversion efficiency of a two-port dual polarized rectenna. Furthermore, [35] applied [32] and presented a formulation deriving the estimated tag range in the case of multi-port (grid) RFID systems.

The received power $P_{r,n}$ at port n is expressed as in [35]

$$P_{r,n} = \left(\frac{\lambda_0}{4\pi R_n}\right)^2 P_t G_t G_{r,n} \tag{5}$$

where $G_{r,n}$ is an embedded realized gain at port n. Setting the received power equal to the threshold power P_{th} to activate the tag chip, and using the definition of the reference range factor R_0, equation (5) can be solved to derive the range of a chip placed at port n

$$\frac{R_n}{R_0} = \sqrt{G_{r,n}} \tag{6}$$

which is similar to (4).

The embedded realized gain $G_{r,n}$ is given by [36]

$$G_{r,n} = 4R_c\,|[\mathbf{Y}]_n \mathbf{g}|^2 \tag{7}$$

where $\mathbf{Y} = (\mathbf{Z_C}+\mathbf{Z_A})^{-1}$ with $\mathbf{Z_A}=\mathbf{R_A}+j\mathbf{X_A}$, the impedance matrix of the n-port (here two-port) antenna system and $\mathbf{Z_C} = Z_c\mathbf{I_n}$ ($\mathbf{I_n}$: the identity matrix of dimension n), the impedance of the RFID chip. The operator $[\mathbf{Y}]_n$ denotes the n-th row (vector) of matrix $\mathbf{Y}$. The definition of $\mathbf{g}$ (column vector of normalized antenna gain) in (7) is slightly different than the one presented in [35] in that it includes a $\sqrt{\eta}$ factor ($\eta = 120\pi$). The elements g_n of column vector $\mathbf{g}$ are proportional to the radiated fields F_n at port n when a unit current excitation is applied at port n with all other ports open.

$$g_n = \sqrt{\frac{4\pi}{\eta}} F_n. \tag{8}$$

Assuming a unit current excitation, the input power at port n is $P_{in,n} = R_{A,nn}/2$. Considering the definition of antenna gain [36], the gain G_n is computed as follows

$$G_n = \frac{4\pi}{\eta R_{A,nn}}\,|F_n|^2 = \frac{|g_n|^2}{R_{A,nn}} \tag{9}$$

$R_{A,nn}$ denotes the self-resistance at port n. Using (9) and (7) one may write (6) as:

$$\frac{R_n}{R_0} = \sqrt{G_n \tau_n} \tag{10}$$

with

$$\tau_n = 4R_c R_{A,nn}\frac{|[\mathbf{Y}]_n\,\mathbf{g}|^2}{|g_n|^2} \tag{11}$$

where τ_n is the power transmission coefficient at port n of the multiport system which describes matching of the antennas

and the excitation ports. One can easily verify that (11) reduces to (2) in the case of a single antenna.

The antenna impedance matrix $\mathbf{Z_A}$ and far-field components F_n and consequently g_n can be obtained for example from a commercial EM simulator considering the tag antenna in the transmitting mode. In the case of the dual tag antenna presented in this paper the matrix $\mathbf{Z_A}$ is not symmetric due to the difference between the sensing and reference tag layouts. The estimated read range of the proposed RFID-enabled sensor tag is shown in Fig. 9. The direction of the arrows indicates the occurrence of the event (before → after). The performance of the sensing tags (dual- and single tag sensors) has significantly affected by the event while the reference tag of the dual tag sensor maintains its performance.

III. Experimental Results

A. Sensor Interrogation

As a proof-of-concept, the designed RFID-based haptic sensor tag was inkjet-printed on a commercially available photopaper (Kodak, USA [37]), which was then sintered at 120 °C for 2 hours as shown in Fig. 6. Its performance was comprehensively measured. The silver nanoparticle ink and the photopaper substrate have been thoroughly studied and their electrical properties are reported in [7] and [15]. The conductivity value of the inkjet-printed silver nanoparticle ink at room temperature after the sintering process at 120 °C is about 2.1×10^6 S/m [7], [15]. The dielectric constant (ε_r) and the loss tangent ($\tan\delta$) of the 254 μm thick (10 mil) photo paper at 915 MHz are about 3.1 and 0.05, respectively [37]. The resolution of the inkjet-printing technology is about 25 μm without any surface treatment, and it is possible to realize about 1 μm resolution by utilizing sub-femtoliter ink droplet [38]. The cost of inkjet-printed RFID tags are analyzed in [40]. The printing resolution of 50 μm (600 dpi) can be robustly obtained with a commercial printer which is sufficient for UHF band antennas because it is less than 1/200 of the wavelength at UHF band (300 MHz ∼ 3 GHz) [#]. The simulated resonant frequencies of the antennas with the fabrication error of 50 μm does not shift more than 1 % from the resonant frequency of the antenna without the fabrication error. The variability of the inkjet printing process does not pose a critical concern in the performance of the sensor. The Voyantic Tagformance reader [40] was utilized in all measurements in the anechoic chamber. A circularly polarized panel antenna which has 8 dBi gain was utilized as the transmission (Tx) antenna of the RFID reader and the distance between the Tx antenna and the fabricated RFID-enabled sensor tag was about 60 cm (2 feet). The required minimum transmitted (Tx) power levels from the reader for the excitation of the RFID tags of the RFID-enabled sensor were recorded and plotted. The resolution of the frequency sweep was 1 MHz and the resolution of the Tx power was 0.1 dB. In this paper, an event occurrence is defined when a finger touches the meandered line of the antenna 1 (sensor tag). The RFID chip was modeled as a series RC network in order to get the RFID chip output impedance of 13-j122Ω at 915 MHz [30]. It would be more preferable to characterize the RFID chip over the frequency range of interest

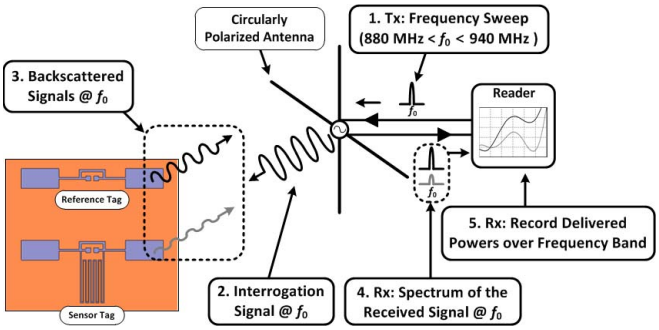

Fig. 10. Measurement procedure.

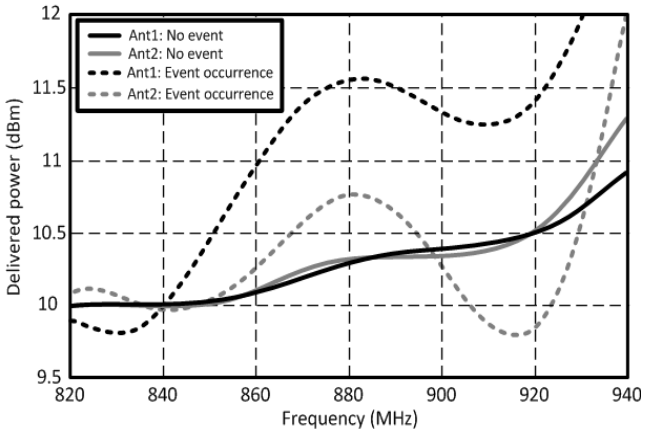

Fig. 11. Delivered power to the each tag (antenna1, antenna2) before/after event occurrence.

to accurately evaluate the exact reflection coefficients of the antennas and the values of the required minimum Tx power.

The measurement setup and procedure are shown in Fig. 10. A narrow band signal is transmitted to the RFID-enabled sensor and backscattered signals from the each tag are recorded at the frequency band of interest (820 MHz ∼ 940 MHz). The whole procedure including frequency sweep and recording the received power takes less than 10 seconds with 1 MHz frequency step when the Voyance Tagformance reader is utilized [40]. The reading time can be reduced by adjusting the resolution of scanning power level and frequency. The received signals from each tag can be distinguished without collision because the reader can handle multiple tags when the RFID system follows EPC Gen2 protocol [41]. The delivered power level at the each antenna was measured as shown in Fig. 11 (5. Rx: Record Delivered Powers over Frequency band in Fig. 10). The RFID-enabled sensor which consists of two RFID tags was interrogated with 30 dBm power (FCC part 15 [43]) and the delivered power to each RFID tag was measured before and after an event occurrence. The delivered power to the antennas was calculated by adding the measured path loss to the measured received power from each tag at the reader. The path loss was measured utilizing a wideband UHF reference RFID tag of the Tagformance reader [40]. The gain of the RFID-enabled sensor is about 3 dBi, the interrogation distance is 0.6 m, and the required minimum power to activate the RFID chip is −15 dBm. A theoretical free space pass loss

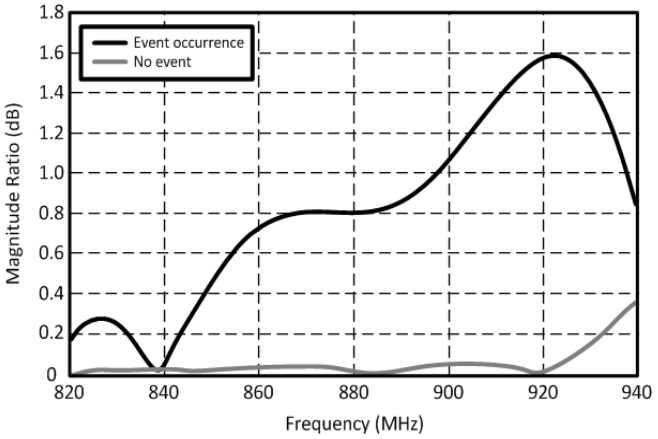

Fig. 12. Magnitude ratio (absolute power level difference) of the antenna 1 (sensor tag) and the antenna 2 (reference tag) before/after the event occurrence.

at 880 MHz is 26.89 dB and the delivered power at the sensor can be calculated using (1) with the link budget. The calculated delivered power at the sensor tag is about 14.11 dBm at the center of the operation frequency range (880 MHz) which is consistent with the data shown in Fig. 11. The received power levels of the backscattered power from each antenna were almost the same when there was no event. However, a significant difference (up to 1.6 dB around 920 MHz) in the backscatter power level of the two antennas of the dual-tag sensor was observed upon the occurrence of an event such as touch. This response successfully demonstrates the feasibility of the proposed differential sensing mechanism through the use of a simple signal process.

B. Detection/Event Decision

An event decision can be made based on the measurement curves shown in Fig. 11. The absolute value of the magnitude difference between the two measured received power level curves after the event occurrence is much higher than that in the absence of any event as shown in Fig. 11 and Fig. 12. For a more accurate event detection, data samples are collected over different frequency points. Each curve shown in Fig. 11 represents a dataset. The data points of each curve are a dataset, and the dataset consists of the measured magnitude of the delivered power to each tag at each frequency. For instance, there are two datasets from the reference tag (solid and dashed gray lines in Fig. 11) and the sensor tag (solid and dashed black lines in Fig. 11), and each dataset has 121 data points because the delivered power has been measured at each frequency (1 MHz frequency step over the frequency range from 820 MHz to 940 MHz). The mean value (μ) and the standard deviation (σ) of the dataset experience significant changes before/after the event occurrence. The mean values (μ) of the datasets before the event occurrence are 10.32 dBm (gray curve in Fig. 11) and 10.29 dBm (black curve in Fig. 11), respectively. The standard deviation (σ) of the datasets before the event occurrence are 0.32 dBm (gray solid curve in Fig. 11) and 0.3 dBm (black solid curve in Fig. 11), respectively. However, the mean values (μ) of the datasets after the event occurrence are 10.31 dBm (gray dashed curve in Fig. 11) and 11.09 dBm (black dashed curve in Fig. 11), respectively. The standard deviation (σ) of the datasets after the event occurrence are 0.52 dBm (gray dashed curve in Fig. 11) and 0.78 dBm (black dashed curve in Fig. 11), respectively. The mean value (μ) and the standard deviation value (σ) of the sampled absolute power level difference curves from the sensor tag (antenna 1) and the reference tag (antenna 2) before the event occurrence results in close values due to the small differences between the received power level curves (gray line in Fig. 12). However, the mean value (μ) and standard deviation (σ) are significantly different after the event occurrence due to the noticeable differences between the power level curves (black line in Fig. 12). The correlation coefficient (ρ) of the two datasets of the recorded (sampled) received power levels by the reader changes dramatically due to the significant changes of the mean values (μ) and standard deviation values (σ) in the event of a touching incident. The Pearson product-moment correlation coefficient of the variable X and Y (PPMCC, $\rho_{X,Y}$), which is commonly used to quantify the degree of the linear dependence and similarity of two variables in a simple way can be calculated as shown in (12) [43]. In addition, the PPMCC value is the same regardless of the magnitude of the curves, enabling a rugged sensing performance that is almost independent from the interrogation range and angle despite the fact that received power levels may vary significantly. It enables robust sensing because the behavior of each tag is independent from the interrogation distance and angle although the received power level may vary depending on those. In this paper, the variable set X is the received power from the sensor tag (antenna 1) and the variable set Y is that from the reference tag (antenna 2) at the reader which are shown in Fig. 11.

$$\rho_{X,Y} = \frac{cov(X,Y)}{\sigma_X \sigma_Y} = \frac{\mathrm{E}\left[(X-\mu_X)(Y-\mu_Y)\right]}{\sigma_X \sigma_Y} \tag{12}$$

where $cov(X, Y)$ is the covariance of the variables X and Y, σ_X and σ_Y are the standard deviation values of the variables X and Y, μ_X and μ_Y are the mean values of the variables X and Y, and E[·] denotes the expectation value of the variable. The coefficient $\rho_{X,Y}$ can take any values between $+1$ and -1 inclusively depending on the similarity of the variables. In case of a discrete dataset, which is the most common data form in most of the sensor systems, the correlation coefficient of (12) can be re-written as the sample correlation coefficient, r, (13) [44].

$$r = \frac{\sum_i^N \left(X_i - \bar{X}\right)\left(Y_i - \bar{Y}\right)}{\sqrt{\sum_i^N \left(X_i - \bar{X}\right)^2}\sqrt{\sum_i^N \left(Y_i - \bar{Y}\right)^2}} \tag{13}$$

where N is the number of the sample dataset, $\bar{X}$ and $\bar{Y}$ are the mean values of the datasets X and Y, respectively. In this paper, the magnitude of the correlation coefficient of the received power level curves can be considered as the similarity of the two curves [43]. The correlation coefficient value is close to $+1$ when the two curves are very similar while the value is getting lower as the absolute difference of the curves increases over the frequency of operation. The minimum required number of the sampled data points can be

estimated based on the confidence interval (β) and the chance of successful event detection (p) as shown in (14) [44].

$$N \geq \frac{\ln(1-\beta)}{\ln(1-p)} \tag{14}$$

In this paper, the 99% of confidence interval and 95 % of successful event detection are assumed and it requires more than 90 sample points which number is smaller than the data points used in calculating correlation coefficient (r). In this work, 121 sample points were used in calculating the correlation coefficient since the resolution of the frequency sweep was 1 MHz. Based on the measurement, the sample correlation coefficient value before an event occurrence was 0.97, while it dropped to 0.68 after event occurrence. The event occurrence decision can be made based on the abrupt change of the sample correlation coefficient at the reader side, with a value around $0.75 \sim 0.85$ can be used as the threshold for the detection.

IV. Conclusion and Future Work

In this paper, a novel inkjet-printed dual-tag RFID-enabled haptic calibration-free sensor with miniaturization/reduced crosstalk enhancing LC resonators, which are embedded in the tag antennas, are introduced on paper substrates. Two RFID tags at 915 MHz are juxtaposed to implement a differential sensing mechanism, which features numerous advantages, including a high event-detection sensitivity as well as performance that is nearly independent from the ambient sensitivity. The differential sensing mechanism utilizing two RFID tags has many advantages such as high sensitivity to ambient environment and mounting substrate, which eliminates the need for time-consuming additional calibration steps. The measured data have verified the "rugged" performance of the proposed RFID-enabled sensor in terms of transmitted/received power level at the RFID reader and the Pearson product-moment correlation coefficient has been utilized to detect and decide a haptic event occurrence (e.g. presence of a human finger).

The future work is to develop a reader to read the proposed RFID-enabled dual tag sensor. The reader for the proposed sensor requires frequency sweep, signal processing, and EPC Gen 2 protocol capability to detect and interrogate the proposed dual tag sensor. Numerous types of sensors (humidity, gas, strain, etc.) can be generated based on the proposed dual tag sensor topology by printing sensing materials on the sensor tag [7], [39], [45]. Large number of sensor tags can be also easily fabricated and deployed due to the repeatability and reliability of the printing technology. The proposed sensor topology could find numerous future applications ranging from Man-to-Machine and Machine-to-Machine (M2M) communications to "smart" agricultural and liquid level and quality monitoring and identification.

References

[1] H. Liu, M. Bolic, A. Nayak, and I. Stojmenovic, "Taxonomy and challenges of the integration of RFID and wireless sensor networks," *IEEE Netw.*, vol. 22, no. 6, pp. 26–35, Nov./Dec. 2008.

[2] R. Want, "An introduction to RFID technology," *IEEE Pervasive Comput.*, vol. 5, no. 1, pp. 25–33, Mar. 2006.

[3] D. Girbau, A. Ramos, A. Lazaro, S. Rima, and R. Villarino, "Passive wireless temperature sensor based on time-coded UWB chipless RFID tags," *IEEE Trans. Microw. Theory Techn.*, vol. 60, no. 11, pp. 3623–3632, Nov. 2012.

[4] R. A. Potyrailo, C. Surman, S. Go, Y. Lee, T. Sivavec, and W. G. Morris, "Development of radio-frequency identification sensors based on organic electronic sensing materials for selective detection of toxic vapors," *J. Appl. Phys.*, vol. 106, no. 12, pp. 124902-1–124902-6. Dec. 2009.

[5] C. Occhiuzzi, C. Paggi, and G. Marrocco, "Passive RFID strain-sensor based on meander-line antennas," *IEEE Trans. Antennas Propag.*, vol. 59, no. 12, pp. 4836–4840, Dec. 2011.

[6] J. Virtanen, L. Ukkonen, T. Bjorninen, A. Z. Elsherbeni, and L. Sydänheimo, "Inkjet-printed humidity sensor for passive UHF RFID systems," *IEEE Trans. Instrum. Meas.*, vol. 60, no. 8, pp. 2768–2777, Aug. 2011.

[7] S. Kim *et al.*, "Inkjet-printed antennas, sensors and circuits on paper substrate," *IET Microw. Antennas Propag.*, vol. 7, no. 10, pp. 858–868, Jul. 2013.

[8] H. Rajagopalan and Y. Rahmat-Samii, "Ingestible RFID bio-capsule tag design for medical monitoring," in *Proc. IEEE Antennas Propag. Soc. Int. Symp. (APS/URSI)*, Toronto, ON, Canada, Jul. 2010, pp. 1–4.

[9] J. Li, Y. Zhang, K. Nagaraja, and D. Raychaudhuri, "Supporting efficient machine-to-machine communications in the future mobile internet," in *Proc. IEEE Wireless Commun. Netw. Conf. Workshops (WCNCW)*, Paris, France, Apr. 2012, pp. 181–185.

[10] A. Gluhak, S. Krco, M. Nati, D. Pfisterer, N. Mitton, and T. Razafindralambo, "A survey on facilities for experimental internet of things research," *IEEE Commun. Mag.*, vol. 49, no. 11, pp. 58–67, Nov. 2011.

[11] S. Kim, Y. Kawahara, A. Georgiadis, A. Collado, and M. M. Tentzeris, "Low-cost inkjet-printed fully passive RFID tags using metamaterial-inspired antennas for capacitive sensing applications," in *Proc. IEEE MTT-S Int. Microw. Symp. (IMS)*, Seattle, WA, USA, Jun. 2013, pp. 1–4.

[12] K. Buell, H. Mosallaei, and K. Sarabandi, "Metamaterial insulator enabled superdirective array," *IEEE Trans. Antennas Propag.*, vol. 55, no. 4, pp. 1074–1085, Apr. 2007.

[13] M. Selvanayagam and G. V. Eleftheriades, "A compact printed antenna with an embedded double-tuned metamaterial matching network," *IEEE Trans. Antennas Propag.*, vol. 58, no. 7, pp. 2354–2361, Jul. 2010.

[14] T. H. J. van Osch, J. Perelaer, A. W. M. de Laat, and U. S. Schubert, "Inkjet printing of narrow conductive tracks on untreated polymeric substrates," *Adv. Mater.*, vol. 20, no. 2, pp. 343–345, Jan. 2008.

[15] L. Yang, A. Rida, R. Vyas, and M. M. Tentzeris, "RFID tag and RF structures on a paper substrate using inkjet-printing technology," *IEEE Trans. Microw. Theory Techn.*, vol. 55, no. 12, pp. 2894–2901, Dec. 2007.

[16] S. Shrestha, M. Balachandran, M. Agarwal, V. V. Phoha, and K. Varahramyan, "A chipless RFID sensor system for cyber centric monitoring applications," *IEEE Trans. Microw. Theory Techn.*, vol. 57, no. 5, pp. 1303–1309, May 2009.

[17] N. Cho, S.-J. Song, S. Kim, S. Kim, and H.-J. Yoo, "A 5.1-μW UHF RFID tag chip integrated with sensors for wireless environmental monitoring," in *Proc. 31st Eur. Solid-State Circuits Conf. (ESSCIRC)*, Sep. 2005, pp. 279–282.

[18] H. Shen, L. Li, and Y. Zhou, "Fully integrated passive UHF RFID tag with temperature sensor for environment monitoring," in *Proc. 7th Int. Conf. ASIC*, Oct. 2007, pp. 360–363.

[19] A. Vaz *et al.*, "Full passive UHF tag with a temperature sensor suitable for human body temperature monitoring," *IEEE Trans. Circuits Syst. II, Exp. Briefs*, vol. 57, no. 2, pp. 95–99, Feb. 2010.

[20] H. Reinisch *et al.*, "A 7.9 μW remotely powered addressed sensor node using EPC HF and UHF RFID technology with -10.3dBm sensitivity," in *IEEE Int. Solid-State Circuits Conf. Dig. Tech. Papers*, Feb. 2011, pp. 454–456.

[21] J. Gao, J. Sidén, H. Nilsson, and M. Gulliksson, "Printed humidity sensor with memory functionality for passive RFID tags," *IEEE Sensors J.*, vol. 13, no. 5, pp. 1824–1834, May 2013.

[22] J. Siden, X. Zeng, T. Unander, A. Koptyug, and H.-E. Nilsson, "Remote moisture sensing utilizing ordinary RFID tags," in *Proc. IEEE Sensors*, Atlanta, GA, USA, Oct. 2007, pp. 308–311.

[23] J. Zhu and G. V. Eleftheriades, "Dual-band metamaterial-inspired small monopole antenna for WiFi applications," *Electron. Lett.*, vol. 45, no. 22, pp. 1104–1106, Oct. 2009.

[24] J. Zhu and G. V. Eleftheriades, "A simple approach for reducing mutual coupling in two closely spaced metamaterial-inspired monopole antennas," *IEEE Antennas Wireless Propag. Lett.*, vol. 9, pp. 379–382, Apr. 2010.

[25] F. W. Grover, *Inductance Calculations: Working Formulas and Tables*. Mineola, NY, USA: Dover, 2004.

[26] R. Esfandiari, D. W. Maki, and M. Siracusa, "Design of interdigitated capacitors and their application to gallium arsenide monolithic filters," *IEEE Trans. Microw. Theory Techn.*, vol. 31, no. 1, pp. 57–64, Jan. 1983.
[27] H. Lee, S. Kim, D. De Donno, and M. M. Tentzeris, "A novel 'Universal' inkjet-printed EBG-backed flexible RFID for rugged on-body and metal mounted applications," in *IEEE MTT-S Int. Microw. Symp. Dig. (MTT)*, Montréal, QC, Canada, Jun. 2012, pp. 1–3.
[28] S.-H. Hwang, T.-S. Yang, J.-H. Byun, and A. S. Kim, "Complementary pattern method to reduce mutual coupling in metamaterial antennas," *IET Microw., Antennas Propag.*, vol. 4, no. 9, pp. 1397–1405, Sep. 2010.
[29] C. Gabriel, "Compilation of the dielectric properties of body tissues at RF and microwave frequencies," Brooks Air Force, San Antonio, TX, USA, Tech. Rep. AL/OE-TR-1996–0037, 1996.
[30] [Online]. Available: http://www.nxp.com/documents/data_sheet/SL3ICS1002_1202.pdf, accessed Nov. 14, 2014.
[31] K. V. S. Rao, P. V. Nikitin, and S. F. Lam, "Antenna design for UHF RFID tags: A review and a practical application," *IEEE Trans. Antennas Propag.*, vol. 53, no. 12, pp. 3870–3876, Dec. 2005.
[32] J. R. Mautz and R. Harrington, "Modal analysis of loaded N-port scatterers," *IEEE Trans. Antennas Propag.*, vol. 21, no. 2, pp. 188–199, Mar. 1973.
[33] R. E. Collin, *Antennas and Radiowave Propagation*. New York, NY, USA: McGraw-Hill, 1985.
[34] A. Georgiadis, G. Andia Vera, and A. Collado, "Rectenna design and optimization using reciprocity theory and harmonic balance analysis for electromagnetic (EM) energy harvesting," *IEEE Antennas Wireless Propag. Lett.*, vol. 9, pp. 444–446, May 2010.
[35] G. Marrocco, "RFID grids: Part I—Electromagnetic theory," *IEEE Trans. Antennas Propag.*, vol. 59, no. 3, pp. 1019–1026, Mar. 2011.
[36] C. A. Balanis, *Antenna Theory: Analysis and Design*, 3rd ed. New York, NY, USA: Wiley, 2005.
[37] [Online]. Available: http://www.kodak.com/, accessed Nov. 14, 2014.
[38] J.-U. Park *et al.*, "High-resolution electrohydrodynamic jet printing," *Nature Mater.*, vol. 6, pp. 782–789, Aug. 2007.
[39] S. Kim *et al.*, "No battery required: Perpetual RFID-enabled wireless sensors for cognitive intelligence applications," *IEEE Microw. Mag.*, vol. 14, no. 5, pp. 66–77, Jul./Aug. 2013.
[40] [Online]. Available: http://www.voyantic.com/tagformance, accessed Nov. 14, 2014.
[41] J. H. Choi, D. Lee, and H. Lee, "Query tree-based reservation for efficient RFID tag anti-collision," *IEEE Commun. Lett.*, vol. 11, no. 1, pp. 85–87, Jan. 2007.
[42] *Understanding the FCC Regulations for Low-Power, Non-Licensed Transmitters*, Federal Commun. Commission, Washington, DC, USA, Feb. 1996.
[43] J. L. Rodgers and W. A. Nicewander, "Thirteen ways to look at the correlation coefficient," *Amer. Statist.*, vol. 42, no. 1, pp. 59–66, Feb. 1988.
[44] R. B. Dell, S. Holleran, and R. Ramakrishnan, "Sample size determination," *ILAR J.*, vol. 43, no. 4, pp. 207–213, Apr. 2002.
[45] L. Yang, R. Zhang, D. Staiculescu, C. P. Wong, and M. M. Tentzeris, "A novel conformal RFID-enabled module utilizing inkjet-printed antennas and carbon nanotubes for gas-detection applications," *IEEE Antennas Wireless Propag. Lett.*, vol. 8, pp. 653–656, Jul. 2009.

Sangkil Kim (S'11) received the B.S. degree in electrical and electronic engineering from Yonsei University, Seoul, Korea, in 2010, and the M.S. and Ph.D. degrees in electrical engineering from the Georgia Institute of Technology, Atlanta, GA, USA, in 2012 and 2014, respectively. He visited the King Abdullah University of Science and Technology (Thuwal, Saudi Arabia, 2013), CTTC (Barcelona, Spain, 2013), and CNRS-LAAS (Toulous, France, 2013) as a Visiting Scholar. He is currently working on the design and fabrication of printed RF energy harvesting-enabled standalone low-power sensor platform.

Yoshihiro Kawahara (S'01–M'06) was born in Tokushima, Japan. He received the B.S. and M.S. degrees in information communication engineering from the University of Tokyo, Tokyo, Japan, in 2000 and 2002, respectively, and the Ph.D. degree in information science and technology from the University of Tokyo, in 2005.

He joined the Graduate School of Information Science and Technology, University of Tokyo, in 2005, as an Assistant Professor and worked on wireless sensing and ubiquitous computing. In 2011, he was a Visiting Scholar at the Georgia Institute of Technology, Atlanta, GA, USA, where he researched a rapid prototyping technology of high-frequency circuits and energy harvesting-enabled electronics devices. He has been an Associate Professor at the University of Tokyo since 2013.

Dr. Kawahara is a member of the IEEE MTT-S TC-24 RFID Technologies and TC-26 Wireless Energy Transfer and Conversion. He serves at the Editorial Board of *Journal on Wireless Power Transfer* (Cambridge). He is a member of IEICE and ACM. His research interests include energy harvesting and ubiquitous computing systems.

Apostolos Georgiadis (S'94–M'03–SM'08) was born in Thessaloniki, Greece. He received the B.S. degree in physics and the M.S. degree in telecommunications from the Aristotle University of Thessaloniki, Thessaloniki, in 1993 and 1996, respectively, and the Ph.D. degree in electrical engineering from the University of Massachusetts, Amherst, MA, USA, in 2002.

He spent a semester with Radio Antenna Communications, Milan, Italy, in 1995, working on Yagi antennas for U.H.F. applications. In 2000, he spent three months with Telaxis Communications, South Deerfield, MA, USA, assisting in the design and testing of a pillbox antenna for LMDS applications. In 2002, he joined Global Communications Devices, North Andover, MA, USA, as a Systems Engineer, and worked on CMOS transceivers for wireless network applications. In 2003, he joined Bermai, Inc., Minnetonka, MN, USA, as an RF/Analog Systems Architect. In 2005, he joined the University of Cantabria, Santander, Spain, as a Juan de la Cierva Fellow Researcher. In 2006, he was a Consultant for Bitwave Semiconductor, Lowell, MA, USA. In addition, he collaborated with ACORDE S.A., Santander, in the design of integrated CMOS VCOs for ultra wideband applications. In 2007, he joined CTTC as a Senior Research Associate in the area of communications subsystems. Since 2013, he has been a Coordinator of the Department of Microwave Systems and Nanotechnology at CTTC.

Dr. Georgiadis received the Fulbright Scholarship for graduate studies at the University of Massachusetts in 1996. He received the Outstanding Teaching Assistant Award from the University of Massachusetts in 1997 and 1998. He was also the recipient of the Eugene M. Isenberg Award from the Isenberg School of Management, University of Massachusetts, in 1999 and 2000. He was the General Chair of 2011 IEEE RFID-TA Conference and General Co-Chair of the 2011 IEEE MTT-S IMWS on Millimeter Wave Integration Technologies. He was the Chairman of the COST Action IC0803 RF/Microwave communication subsystems for emerging wireless technologies. He is a Coordinator of Marie Curie Industry-Academia Pathways and Partnerships Project Symbiotic Wireless Autonomous Powered system. He is the Chair of the IEEE MTT-S TC-24 RFID Technologies and member of the IEEE MTT-S TC-26 Wireless Energy Transfer and Conversion. He serves at the Editorial Board of the *Radioengineering* journal and as an Associate Editor of the IEEE MICROWAVE AND WIRELESS COMPONENTS LETTERS and *IET Microwaves, Antennas and Propagation* Journals.

Ana Collado (M'07–SM'12) was born in Santander, Spain. She received the B.S. degree in telecommunications engineering and the Ph.D. degree from the University of Cantabria, Santander, in 2002 and 2007, respectively. In 2002, she was with the University of the Basque Country, Bilbao, Spain, studying the uncertainty in the noise figure measurements in monolithic microwave integrated circuit low-noise amplifiers. Since 2007, she has been a Research Associate with the Centre Tecnològic de Telecomunicacions de Catalunya, Castelldefels, Spain, in the area of communication subsystems. She was the 2011 Marie Curie Fellow Researcher for Project EU FP7-251557 Symbiotic Wireless Autonomous Powered System, and a Management Committee Member and Grant Holder Representative of EU COST Action IC0803, and RF/Microwave communication subsystems for emerging wireless technologies.

Her areas of interests include the development of techniques for practical bifurcation control and stability analysis of power amplifiers and coupled oscillator systems, and RFID technology, energy harvesting, and wireless power transmission solutions.

Manos M. Tentzeris (S'89–M'92–SM'03–F'10) received the Diploma (*magna cum laude*) degree in electrical and computer engineering from the National Technical University of Athens, Athens, Greece, and the M.S. and Ph.D. degrees in electrical engineering and computer science from the University of Michigan, Ann Arbor, MI, USA. He is currently a Professor with the School of Electrical and Computer Engineering, Georgia Institute of Technology (Georgia Tech), Atlanta, GA, USA. He has authored over 420 papers in refereed journals and conference proceedings, five books, and 19 book chapters. He has helped develop academic programs in Highly Integrated/Multilayer Packaging for RF and Wireless Applications using ceramic and organic flexible materials, paper-based RFIDs and sensors, biosensors, wearable electronics, inkjet-printed electronics, Green electronics and power scavenging, nanotechnology applications in RF, microwave MEMs, SOP-integrated (UWB, multiband, mmW, and conformal) antennas, and adaptive numerical electromagnetics (FDTD and multiresolution algorithms), and heads the ATHENA Research Group (20 researchers).

He is currently the Head of the Electromagnetics Technical Interest Group with the School of Electrical and Computer Engineering, Georgia Tech, where he served as an Associate Director of RFID/Sensors Research with the Georgia Electronic Design Center from 2006 to 2010, and an Associate Director of RF Research with the NSF-Packaging Research Center and the RF Alliance Leader from 2003 to 2006. He was the recipient/co-recipient of the 2012 FiDiPro Professorship in Finland, the 2010 IEEE Antennas and Propagation Society Piergiorgio L. E. Uslenghi Letters Prize Paper Award, the 2011 International Workshop on Structural Health Monitoring Best Student Paper Award, the 2010 Georgia Tech Senior Faculty Outstanding Undergraduate Research Mentor Award, the 2009 IEEE TRANSACTIONS ON COMPONENTS AND PACKAGING TECHNOLOGIES Best Paper Award, the 2009 E. T. S. Walton Award from the Irish Science Foundation, the 2007 IEEE APS Symposium Best Student Paper Award, the 2007 IEEE IMS Third Best Student Paper Award, the 2007 ISAP 2007 Poster Presentation Award, the 2006 IEEE MTT Outstanding Young Engineer Award, the 2006 Asian-Pacific Microwave Conference Award, the 2004 IEEE TRANSACTIONS ON ADVANCED PACKAGING Commendable Paper Award, the 2003 NASA Godfrey Art Anzic Collaborative Distinguished Publication Award, the 2003 IBC International Educator of the Year Award, the 2003 IEEE CPMT Outstanding Young Engineer Award, the 2002 International Conference on Microwave and Millimeter-Wave Technology Best Paper Award (Beijing, China), the 2002 Georgia Tech-Electrical and Computer Engineering Outstanding Junior Faculty Award, the 2001 ACES Conference Best Paper Award, the 2000 NSF CAREER Award, and the 1997 Best Paper Award of the International Hybrid Microelectronics and Packaging Society. He was the TPC Chair of the IEEE IMS 2008 Symposium and the Chair of the 2005 IEEE CEM-TD Workshop, and is the Vice-Chair of the RF Technical Committee (TC16) of the IEEE CPMT Society. He is the Founder and Chair of the RFID Technical Committee (TC24) of the IEEE MTT Society and the Secretary/Treasurer of the IEEE C-RFID. He is the Associate Editor of the IEEE TRANSACTIONS ON MICROWAVE THEORY AND TECHNIQUES, the IEEE TRANSACTIONS ON ADVANCED PACKAGING, and *International Journal on Antennas and Propagation*. He was a Visiting Professor with the Technical University of Munich, Munich, Germany, for the summer of 2002, GTRI-Ireland, Athlone, Ireland, for the summer of 2009, and LAAS-CNRS, Toulouse, France, for the summer of 2010. He has given over 100 invited talks to various universities and companies all over the world. He is a member of URSI-Commission D and MTT-15 Committee, an Associate Member of EuMA, a fellow of the Electromagnetic Academy, and a member of the Technical Chamber of Greece. He is one of the IEEE MTT-S Distinguished Microwave Lecturers from 2010 to 2012.